JACS
JOURNAL OF THE AMERICAN CHEMICAL SOCIETY
Article
pubs.acs.org/JACS

Rotating Phenyl Rings as a Guest-Dependent Switch in Two-Dimensional Metal–Organic Frameworks

Christopher R. Murdock,[†] Nicholas W. McNutt,[‡] David J. Keffer,[§] and David M. Jenkins*[,†]

[†]Department of Chemistry, [‡]Department of Chemical and Biomolecular Engineering, and [§]Department of Materials Science and Engineering, University of Tennessee, Knoxville, Tennessee 37996-1600, United States

Supporting Information

ABSTRACT: A semirigid bis(1,2,4-triazole) ligand binds in a syn conformation between copper(I) chains to form a series of two-dimensional metal–organic frameworks that display a topology of fused one-dimensional metal–organic nanotubes. These anisotropic frameworks undergo two different transformations in the solid state as a function of solvation. The 2D sheet layers can expand or contract, or, more remarkably, the phenyl rings can rotate between two distinct positions. Rotation of the phenyl rings allows for the adjustment of the tube size, depending on the guest molecules present. This "gate" effect along the 1D tubes has been characterized through single-crystal X-ray diffraction. The transformations can also be followed by powder X-ray diffraction (PXRD) and solid-state ^{13}C cross-polarization magic-angle-spinning (CP-MAS) NMR. Whereas PXRD cannot differentiate between transformations, solid-state ^{13}C CP-MAS NMR can be employed to directly monitor phenyl rotation as a function of solvation, suggesting that this spectroscopic method is a powerful approach for monitoring breathing in this novel class of frameworks. Finally, simulations show that rotation of the phenyl ring from a parallel orientation to a perpendicular orientation occurs at the cost of framework–framework energy and that this energetic cost is offset by stronger framework–solvent interactions.

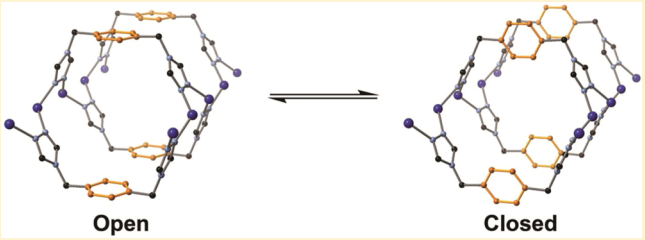

1. INTRODUCTION

Since breathing metal–organic frameworks (MOFs) can switch between opened and closed configurations, these advanced materials have been proposed for applications such as gas separations,[1−10] liquid separations,[1,3,9,10] chemical sensing,[2−7,9−11] and even hazardous waste adsorption.[5,9,12] The existence of multiple stable states combined with fine-tuning of the pore properties allows breathing MOFs to exhibit highly selective guest adsorption.[13−16] Guest-selective pore opening and stepwise adsorption as a function of pressure or concentration result in pore properties that can be modified, leading to an increased interest in the synthesis of additional breathing MOF systems.[5,6,17] Since breathing MOFs are multipurpose porous materials with numerous potential applications, the development of rational synthetic methodologies for their preparation is indispensable.

One constructive approach for designing breathing MOFs begins by determining where the hinge or "kneecap" in the porous material should be placed.[3,7] Kitagawa proposed a system for three-dimensional (3D) materials wherein the dimension of porosity could be either 1D (tubes), 2D (sheets), or 3D (interpenetrated).[18] Of the breathing MOFs that fall within this classification, most flex at the metal–ligand interface, which means that the exact interaction between the ligand and the metal determines whether the MOF can flex.[3,7,10] To avoid this limitation in the synthesis of breathing MOFs, researchers have investigated routes that move the kneecap away from the metal–ligand interface to the ligand itself. Wang, Oliver, and Vittal have independently demonstrated that double-hinged ligands can act like a screw to pull the layers in 2D MOFs together as a function of guest (Figure 1 top), while our research has shown the same screwlike effect with 1D rhombic pores that allows the rhombus to be pinched shut as a function of guest (Figure 1 middle).[19−22] Placing the kneecap solely on the ligand allows for fixed metal–ligand binding points, but it is clear from the dearth of examples that a more robust synthetic strategy is required.

An alternative approach to building breathing MOFs whose kneecap is located solely on the ligand involves preparing an anisotropic framework wherein a moiety of the linker can swivel to block the pore as a function of guest. The concept of applying linker rotation to block the pore has been implied with the development of frameworks in which a subunit of the linker can undergo free rotation.[1,2,23−25] However, to form a breathing MOF, the linker must rotate between fixed positions that would allow for a more effective "gate" effect to occur as the pore is opened and closed. A depiction of an anisotropic metal–organic framework that demonstrates this gate effect is shown in the bottom panel of Figure 1. This gate-opening effect would not be dependent on the metal centers and would potentially allow for a wide range of pore sizes to be synthesized in a highly isoreticular manner with only modest changes to the swiveling subunit. Another advantage of

Received: August 27, 2013
Published: December 18, 2013

   dx.doi.org/10.1021/ja4088709 | J. Am. Chem. Soc. 2014, 136, 671−678

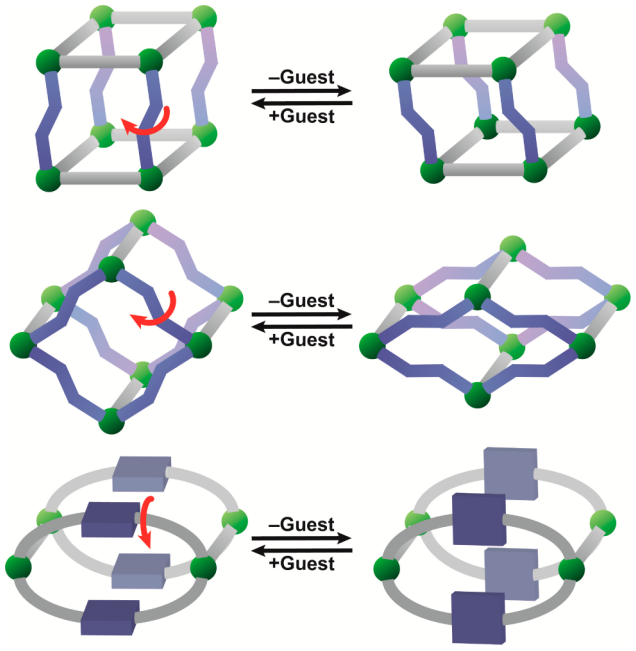

Figure 1. Graphical depiction of methods in which the "kneecap" is placed solely on the ligand. Double-hinged ligands can be used to pull together rigid 2D sheets (top) or 1D chains (middle), or a subunit of the ligand can rotate to open and close the pore (bottom). Green spheres represent metal centers or secondary building units (SBUs), and gray and blue components represent rigid and flexible portions of the ligand, respectively.

employing a gate mechanism is that the rotating subunit may be able to be monitored directly through solid-state spectroscopic methods, such as ^{13}C cross-polarization magic-angle-spinning (CP-MAS) NMR spectroscopy, which is a boon when crystallographic data are not available.

While aryl rings are an obvious component of the rotating gate, only a limited number of examples have been reported to date. Kitagawa and co-workers prepared a pillared-layer cadmium coordination polymer wherein the aryl ring could rotate as a function of hydration, as determined by single-crystal X-ray diffraction (XRD). However, the total motion between the open and closed states of their framework is quite complex because upon dehydration the gate closes concurrently with a contraction of the distance between the layers.[26] More recently, Yang, Schröder, and co-workers prepared a cobalt MOF exhibiting adsorption isotherms consistent with breathing. On the basis of grand canonical Monte Carlo simulations, powder XRD (PXRD), and IR experiments, they concluded that the pyridyl rings in their linkers rotate in the presence of CO_2 to open the channels.[27] To date, a rotating-gate framework in which rotation is solely at the aryl unit has not been fully characterized both by single-crystal XRD and additional spectroscopic methods.

We have synthesized a 2D copper sheet MOF that has a topology of 1D nanotubes fused along the copper chains. The backbone of the framework is formed by a bidentate semirigid linker in a syn conformation whose phenyl subunit rotates between parallel and perpendicular positions as a function of guest solvent. These phenyl rotations open and close the 1D tubes. Crucially, each orientation of the phenyl ring has been confirmed by single-crystal and powder XRD, and more notably, the rotating-gate effect has been observed for the first time by ^{13}C CP-MAS NMR spectroscopy. This direct spectroscopic technique could be highly valuable for testing additional MOFs that breathe by the same gate-rotating mechanism, reducing the need for single-crystal XRD to prove the existence of each state. In addition to experimental measurements, classical molecular dynamics (MD) simulations were conducted on each framework to probe the energetics of this novel breathing motif. The simulations confirmed that each guest favors a different orientation as a result of differences between the energies of the solvent and the framework lattice.

2. RESULTS AND DISCUSSION

2.1. Synthesis of Ligand and Frameworks. We previously reported the synthesis of a semirigid bis(1,2,4-triazole) ligand containing a 2-butene subunit[28] and have expanded this methodology to incorporate a central xylene moiety. Following the method of Horváth,[29] the addition of 1,2,4-triazole-1-propanenitrile to 1,4-bis(bromomethyl)benzene led to the formation of intermediate **1** in 94% yield (Scheme 1).

Scheme 1. Synthesis of Bis(triazole) Ligand, L (2)

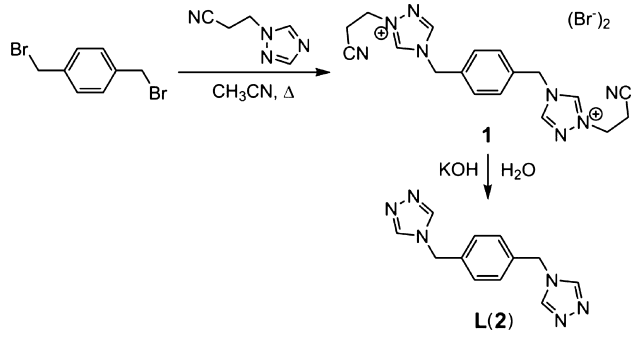

Subsequent cleavage of the propanenitrile group with potassium hydroxide yielded the product 4,4′-(1,4-(xylene)-diyl)bis(1,2,4-triazole), **L** (**2**), in 84% yield. The ligand **L** was further purified via recrystallization from water.

Our previously published results with the semirigid linker 4,4′-(1,4-(*trans*-2-butene)diyl)bis(1,2,4-triazole) demonstrated that it is possible to prepare multiple copper MOFs by varying the reaction conditions, including solvent, metal-to-ligand ratio, and starting metal salt.[19,28] To canvas the reaction space of this new double-hinged ligand **2**, several different reaction conditions were attempted (Scheme 2).

The addition of 1 equiv of both **L** and copper perchlorate to a mixture of *N*,*N*-dimethylformamide (DMF) and water led to the formation of $[Cu(\mathbf{L})(ClO_4)]\cdot DMF\cdot H_2O$ (**3**) (Scheme 2 top). Colorless crystalline needles suitable for X-ray diffraction

Scheme 2. Synthesis of Copper Frameworks Utilizing Various Solvents and Metal-to-Ligand Ratios

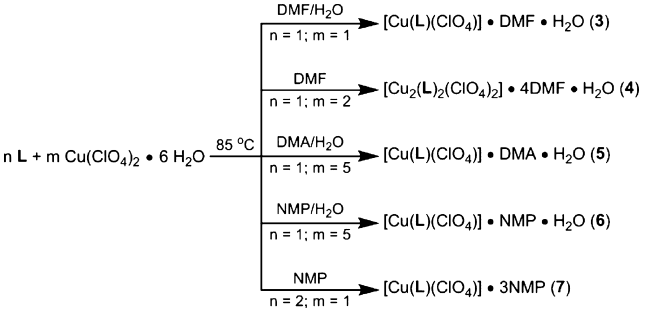

dx.doi.org/10.1021/ja4088709 | J. Am. Chem. Soc. 2014, 136, 671–678

were obtained after heating the reaction mixture for 24 h at 85 °C. Single-crystal XRD showed that each tetrahedral Cu(I) center is coordinated to four triazole ligands (Figure 2A).

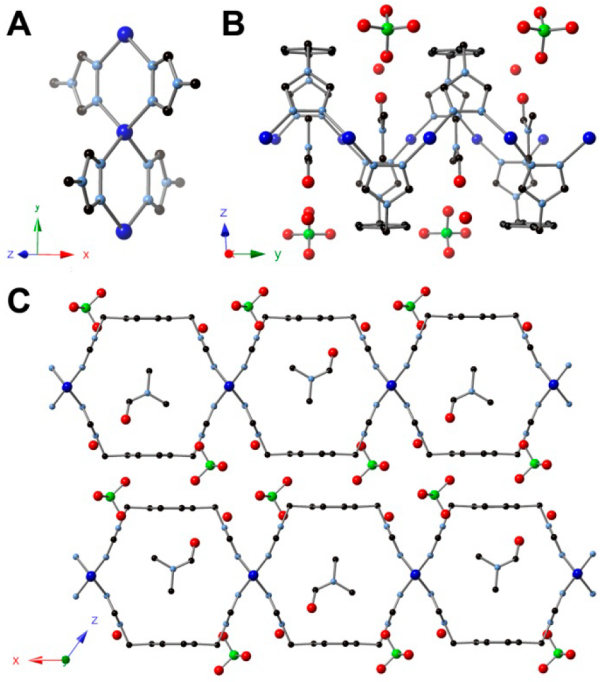

Figure 2. (A) Crystal structure of **3** showing the copper connectivity. (B) Crystal structure of **3** showing copper chains along the *y* axis. (C) Crystal structure of **3** viewed orthogonal to the *y* axis showing the fused-tube topology. Blue, light-blue, black, green, and red spheres represent Cu, N, C, Cl, and O, respectively. All hydrogen atoms have been omitted for clarity.

Adjacent copper atoms are bridged by two triazole ligands to form an equatorial plane, resulting in the formation of a linear chain (Figure 2B). The semirigid ligand exhibits a syn conformation to form a 2D layered structure with neighboring copper chains (Figure 2C).[8,30] Since the triazole ligands bridge the copper centers in an alternating manner, the overall topology is a 2D sheet (Figure 2C). Guest DMF molecules fill the pores of the framework, while the perchlorate anions are packed between the sheet layers.

While framework **3** resembles a 2D network, the actual connectivity does not resemble a 2D square grid.[31,32] The topology is more comparable to a set of fused 1D metal–organic nanotubes (MONTs)[33−36] because of the existence of channels along the *y* axis (Figure 2C). The result of this topology is an anisotropic framework in which porosity is controlled through the size of the 1D pores. The size of these pores are in turn set by the size and shape of the syn-conformed ligand.

By the use of DMF as a solvent and a 2:1 metal-to-ligand ratio, a variant of **3** was obtained. The framework, $[Cu_2(\mathbf{L})_2(ClO_4)_2]\cdot 4DMF\cdot H_2O$ (**4**), was collected as colorless needles after heating in DMF at 85 °C for 36 h (Scheme 2). The crystalline needles are in the same *C*2/*m* space group as **3**, but an increase in the unit cell volume was observed. Crystallographic studies revealed the same connectivity with Cu(I) centers bridged by triazole ligands, resulting in a fused 1D MONT structure similar to that of **3** (Figure S1 in the Supporting Information). While DMF molecules remain within the voids as in **3**, additional DMF molecules are now located between the layers. The $\pi-\pi$ interactions are disrupted in order to accommodate the additional guest molecules, which increases the distance between the layers from 3.8 to 7.3 Å (Figure S1).

As part of our screening of reaction conditions as a function of solvent, we employed structurally similar *N*,*N*-dimethylacetamide (DMA) as a cosolvent with water in the framework reaction. Upon the addition of 1 equiv of **L** to 5 equiv of copper perchlorate, $[Cu(\mathbf{L})(ClO_4)]\cdot DMA\cdot H_2O$ (**5**) was obtained as colorless needles after heating for 2 weeks at 85 °C (Scheme 2). The structure of **5** was topologically identical to that of 3—consisting of Cu(I) centers bridged by two triazole ligands to form a fused-tube structure—but there was one major structural change (Figure 3): the orientation of the phenyl

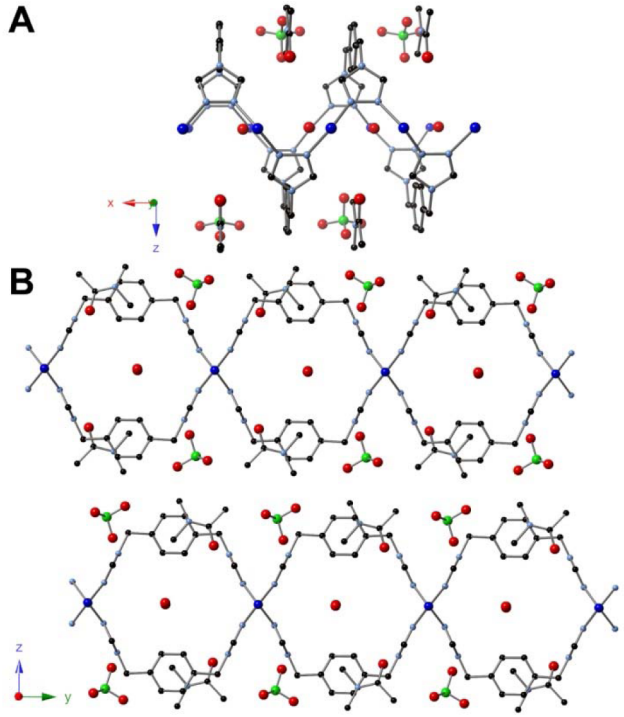

Figure 3. (A) Crystal structure of **5** showing copper chains along the *x* axis. (B) Crystal structure of **5** viewed orthogonal to the *x* axis showing the fused-tube topology.

ring had rotated 90° compared to that in **3**! Whereas the phenyl rings are parallel to one another in **3**, resulting in layers that are stacked through $\pi-\pi$ interactions, the phenyl moieties in **5** are perpendicular to the orientation of the tubes. This rotation of the phenyl rings breaks the $\pi-\pi$ interactions and allows for a migration of the solvent from within the pore to between the rotated phenyl rings (Figures 2 and 3). Despite repeated efforts, we were unsuccessful in preparing a bulk quantity of framework **5**.

Even though framework **5** was not isolable, the existence of the phenyl ring in a perpendicular rather than parallel fashion piqued our interest in synthesizing additional 2D fused MONTs. Although dynamic transformations within MOFs have been studied, including the continuous rotation of phenyl rings,[23−25] the ability to control the rotation between two fixed states would provide a valuable gating technique for porous materials. The ability to switch between different states is beneficial only if the framework is anisotropic, and the existence

dx.doi.org/10.1021/ja4088709 | J. Am. Chem. Soc. 2014, 136, 671−678

of 1D pores in frameworks **3**–**5** provides an ideal platform to study switchable phenyl rotation that can change the pore size.

Given the differences in frameworks **3** and **5**, we desired to attempt to synthesize two frameworks that contain the *same* solvent and show both aryl ring positions. *N*-Methyl-2-pyrrolidone (NMP) was used as a reaction medium to synthesize additional frameworks because of its structural similarity to DMF and DMA. With a combination of NMP and water, $[Cu(\mathbf{L})(ClO_4)]\cdot NMP\cdot H_2O$ (**6**) was obtained after 2 weeks of heating at 85 °C with a metal-to-ligand ratio of 5:1 (Scheme 2). The topologically similar framework again crystallized in the *C*2/*m* space group and is analogous to that of **3**, except that the DMFs within the pores are now replaced with guest NMP molecules (Figure 4). The phenyl moiety remained oriented in a parallel fashion, showing $\pi-\pi$ stacking between the layers with a layer distance of 3.8 Å.

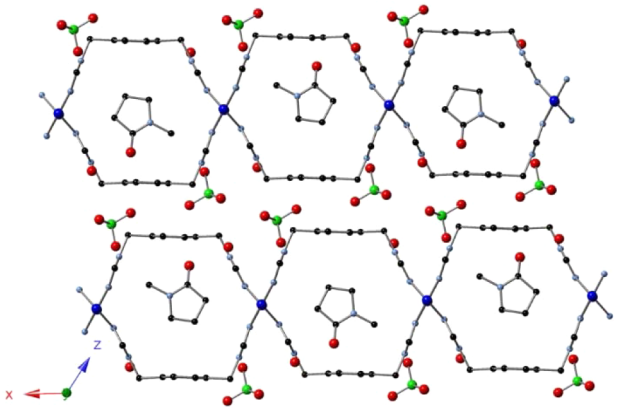

Figure 4. Crystal structure of **6** viewed orthogonal to the *y* axis showing the fused-tube topology.

When only NMP was used as a reaction solvent with a 2:1 ligand-to-metal ratio, $[Cu(\mathbf{L})(ClO_4)]\cdot 3NMP$ (**7**) was formed as colorless needles after 3 days of heating at 85 °C (Scheme 2). Crystallographic studies revealed that the framework crystallizes in the $P\bar{1}$ space group and that the connectivity resembles the previously described frameworks **3**–**6**. Notably, the phenyl moiety is rotated 76° compared with that in **6** (Figure 5). In a similar manner to **5**, the guest NMP molecules are now located between the rotated phenyl rings as well as within the tubular pores. Examination of the estimated pore sizes in frameworks **6** and **7** yields dimensions of 9.0 Å × 10.5 Å for **6** and 4.9 Å × 10.7 Å for **7**.

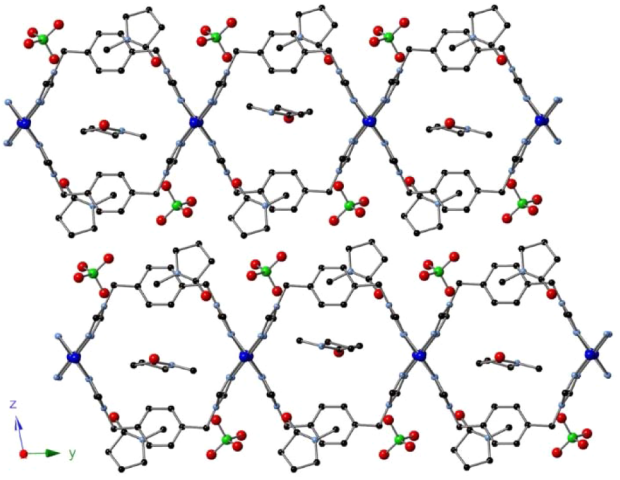

Figure 5. Crystal structure of **7** viewed orthogonal to the *x* axis showing the fused-tube topology.

The synthesis of **7** demonstrates that we were able to prepare a pair of anisotropic frameworks in which the phenyl moiety exists in two distinct orientations while containing the *same* solvent, NMP, within the lattice. The only variation between frameworks **6** and **7** with regard to elemental composition is that **6** has one guest water molecule while **7** has two additional NMPs. Since the phenyl moiety can crystallographically exist in two distinct positions, the ability to switch the phenyl orientation as a function of solvation is clearly plausible. Nevertheless, for this pore-gating effect to be practical, an in situ monitoring technique that does not rely on single-crystal XRD had to be developed.

2.2. Dynamic Transitions in the Solid State. Once an assortment of isoreticular systems had been synthesized, the next step was to determine whether transitions could occur in the solid state as a function of solvation. Two pairs of frameworks and their transitions could be monitored: **4** to **3** and **7** to **6** (Scheme 3). The first pair features a separation of the 2D sheet layers, while the second pair involves the rotation of the phenyl ring that makes up the backbone of the 1D tubular topology. Although single-crystal X-ray analysis can confirm which state a breathing MOF is in for one crystal, PXRD measurements are commonly employed to investigate transformations to the bulk material.[26,37−39]

Scheme 3. Conversion between Framework States as a Function of Solvent

$$[Cu_2(\mathbf{L})_2(ClO_4)_2]\cdot 4DMF\cdot H_2O\ (\mathbf{4}) \xrightarrow{H_2O,\ rt} [Cu(\mathbf{L})(ClO_4)]\cdot DMF\cdot H_2O\ (\mathbf{3})$$

$$[Cu(\mathbf{L})(ClO_4)]\cdot 3NMP\ (\mathbf{7}) \underset{NMP/85\ ^\circ C}{\overset{H_2O,\ rt}{\rightleftharpoons}} [Cu(\mathbf{L})(ClO_4)]\cdot NMP\cdot H_2O\ (\mathbf{6})$$

The first pair of frameworks investigated was **3** and **4**, which contain different amounts of DMF in their formulas, causing expansion or contraction of the sheet layers (Scheme 2, Figure 2 and Figure S1 in the Supporting Information). Since **3** and **4** have distinct PXRD patterns (Figures S6 and S7 in the Supporting Information), an experiment that monitored the dynamic transformation as a function of solvent was possible. PXRD patterns were collected on the two powder samples: an as-synthesized sample of **4** and a sample of **4** that was soaked in water for 1 h prior to PXRD analysis (Figure S10 in the Supporting Information). The PXRD patterns were matched with simulated spectra to confirm the phase purity before and after addition of solvent. As expected, the spacing between the 2D sheets could be monitored with PXRD.

The ability to monitor phenyl rotation as a function of solvent with PXRD is of greater interest. Monitoring the rotation of the phenyl rings by PXRD was tested by taking X-ray measurements on three samples: an initial sample of **7**, a hydrated sample of **7** that was first soaked in water and subsequently soaked in a water/NMP mixture, and a sample that was resoaked in pure NMP and heated to 85 °C for 8 h (Figure S11 in the Supporting Information). The PXRD measurements confirmed that the bulk material was transformed from **7** to **6** and back to **7**.

dx.doi.org/10.1021/ja4088709 | *J. Am. Chem. Soc.* 2014, 136, 671−678

Although PXRD measurements confirmed that transformations between the different states occur for these sheet MOFs, an alternative spectroscopic technique, solid-state NMR spectroscopy, can provide more useful information for monitoring dynamic transitions in the solid state. Solid-state NMR spectroscopy has been used extensively to characterize MOFs,[40,41] and in particular, it is a powerful tool for the determination of rotation rates of aryl rings.[23−25] The rotation of aryl rings to locked positions, therefore, offers an ideal case for demonstrating the efficacy of this technique.

Nevertheless, solid-state ^{13}C CP-MAS NMR spectroscopy has rarely been employed to effectively monitor the transition between fixed positions in breathing MOFs.[42−44] In two instances, the twisting motions at metal−ligand kneecaps (and the accompanying aryl rings) in zinc MOFs have been observed as a function of guest.[43,44] The resonances either shift as a function of breathing state or, more constructively, split into multiple resonances as the carbon atoms are rendered inequivalent in their new conformation. However, no ^{13}C CP-MAS NMR measurements have been performed where the breathing motion occurs solely on the ligand.

Prior to the collection of solid-state ^{13}C CP-MAS NMR spectra of the frameworks, it was critical to assign appropriate peak positions for **2** in the solution-state NMR spectrum. Heteronuclear single-quantum coherence (HSQC) and heteronuclear multiple-bond correlation (HMBC) spectra were collected for **2** in DMSO-d_6 along with 1D ^{1}H and ^{13}C NMR spectra, which allowed for absolute assignments of all of the distinct carbons on the ligand (Figures S12−S15 in the Supporting Information). The central aryl carbons have a resonance at 128.16 ppm and the ipso carbons have a resonance at 136.54 ppm in the solution NMR spectrum. These resonances were also confirmed by the ^{13}C CP-MAS NMR spectrum of **2** (Figure S16 in the Supporting Information).

Once the ^{13}C NMR spectrum of **2** had been assigned, we could compare it to the solid-state ^{13}C CP-MAS NMR spectra of the frameworks. A spectrum of **3**, including a portion of the structure and a blow-up of the aryl region, are shown in Figure 6. The resonance at 49.3 ppm is attributed to the methylene carbon of the triazole ring, while the resonances at 131.0, 132.5, 136.0, 136.6, and 144.8 ppm are assigned to the aryl carbons. Although ligand **2** is highly symmetric in solution, the symmetry of the aryl carbons is lost in the solid state because of the different local environments of the aryl atoms. This break in symmetry is due to the solvent and anion molecules within the framework.

Framework solvent can also be located via NMR analysis, and this is a powerful tool for monitoring phase transitions as a function of solvation.[43,44] The solid-state ^{13}C CP-MAS NMR spectrum of **3** shows three peaks for DMF (Figure 6). These correspond to the DMF molecules that are present in the 1D channels. A comparison of the spectra of **3** and **4** shows that there is no significant difference in the aryl region of the spectrum, but an additional set of DMF peaks are observed at 35.5, 39.6, and 166.9 ppm (Figure S17 in the Supporting Information). These additional resonances are due to the presence of two DMF molecules that exhibit different local environments, one contained within the pore and one between the layers.

Analysis of the solid-state NMR spectra for frameworks **6** and **7** allowed us to correlate the peak positions with rotation of the aryl ring in the solid state. The ^{13}C CP-MAS NMR spectrum of

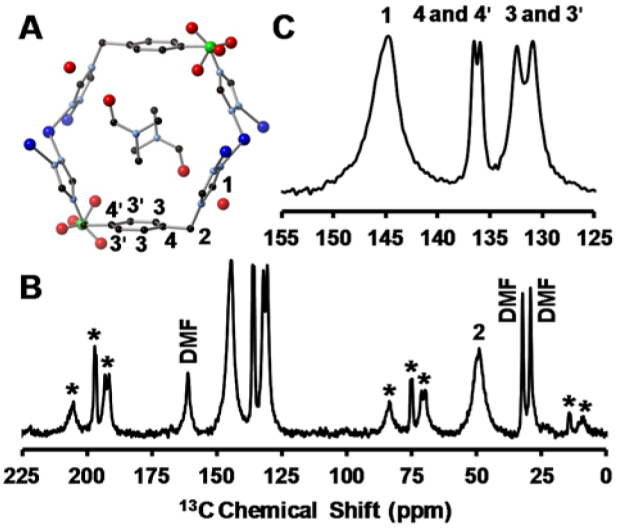

Figure 6. (A) Highlighted portion of the crystal structure of **3** with labeled carbon atoms. (B) Full solid-state ^{13}C CP-MAS NMR spectrum of **3**. Asterisks denote spinning sidebands. (C) Highlight of the aryl region of the spectrum of **3** with labeled peaks.

6 is similar to that of **3**, with the aryl carbons yielding four peaks at 131.7, 133.4, 135.3, and 136.7 ppm as a result of a break in symmetry (Figure 7). Despite a change in solvent in

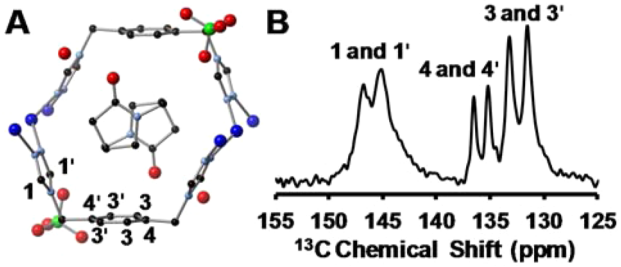

Figure 7. (A) Highlighted portion of the crystal structure of **6** with labeled carbon atoms. (B) Highlight of the aryl region of the solid-state ^{13}C CP-MAS NMR spectrum of **6** with labeled peaks.

the tubular pore, there is little change in peak position of the aryl-ring resonances. The triazole and methylene carbons both exhibit two peaks each, at 46.6 and 49.8 ppm and 145.3 and 146.9 ppm, respectively (Figure 7 and Figure S18 in the Supporting Information), whereas in **3** only one peak is present for each carbon. The triazole and methylene carbons exhibit two separate resonances because there is a slight tilt of the ligand from right to left (Figure 4), causing each individual pore and, ultimately, the ligand to be asymmetric.

When analyzed by ^{13}C CP-MAS NMR spectroscopy, framework **7** exhibits a single broad peak for the methylene and triazole carbons with resonances at 49.7 and 146.6 ppm, respectively, which is in contrast to the results for **6** (Figure 8 and Figure S19 in the Supporting Information). The resonances for the aryl carbons are now at 125.9 (broad), 135.9, and 137.0 ppm. The broad resonance at 125.9 ppm corresponds to the now four inequivalent "3" carbons in the phenyl ring. This increased ring heterogeneity, combined with a possible increase in the chemical shift distribution, leads to this broader peak. Notably, the peaks for the 4 and 4′ carbons have barely shifted between **6** and **7**. The only significant change to the solid-state NMR spectrum involves the resonances

dx.doi.org/10.1021/ja4088709 | J. Am. Chem. Soc. 2014, 136, 671−678

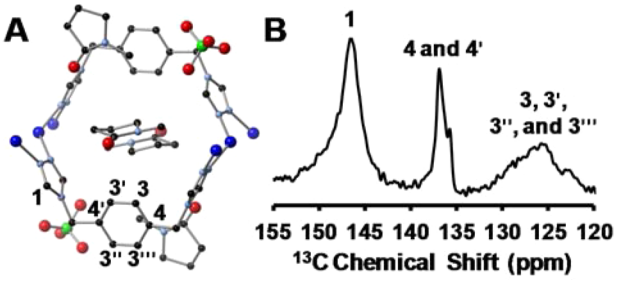

Figure 8. (A) Highlighted portion of crystal structure of **7** with labeled carbon atoms. (B) Highlight of the aryl region of the solid-state ^{13}C CP-MAS NMR spectrum of **7** with labeled peaks.

correlated to the aryl carbons that moved with the framework, which demonstrates that solid-state NMR analysis can differentiate between different breathing modes for the bulk material.

In addition to evaluating the pure-phase frameworks by solid-state NMR spectroscopy, we monitored the changes in the frameworks as a function of solvation. A solid-state ^{13}C CP-MAS NMR spectrum of a sample of **4** was collected, and the sample was then soaked in water for 1 h. The ^{13}C CP-MAS NMR spectrum of hydrated **4** was collected and compared with that of isolated **3**. A match between the spectra of isolated **3** and hydrated **4** was obtained (Figure S20 in the Supporting Information), demonstrating that NMR analysis was successful in monitoring breathing of the framework.

To monitor aryl rotation between **7** and **6**, the solid-state ^{13}C CP-MAS NMR spectrum of a freshly prepared sample of **7**, which had been verified by PXRD, was collected. The sample was subsequently soaked in water for 1 h, and a second NMR spectrum was collected (Figure 9). The spectrum of hydrated **7** was compared to the ^{13}C CP-MAS NMR spectrum of pure **6**, and the two spectra were found to be identical. The same sample of hydrated **7** (i.e., **6**) was therefore soaked in NMP in an attempt to reproduce framework **7**. Although soaking in NMP under ambient conditions did not reproduce **7**, heating the sample at 85 °C for 8 h resulted in an NMR spectrum that

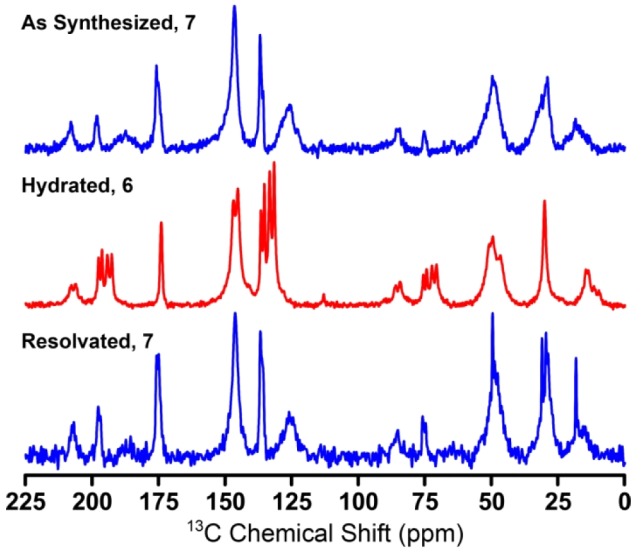

Figure 9. ^{13}C CP-MAS NMR spectra of **7** (top) as-synthesized, (middle) after exposure to water for 1 h, and (bottom) after resolvation with NMP for 8 h at 85 °C.

was a direct match with that of the as-synthesized framework **7** (Figure 9). These experiments demonstrate that ^{13}C CP-MAS NMR spectroscopy is an effective technique to monitor framework breathing in the solid state.

2.3. Simulations of the 2D Frameworks. To assist in understanding how small changes in solvent conditions could twist the phenyl ring between parallel and perpendicular modes in the framework, we turned to simulations of the MOFs. We sought to answer two questions. First, when the simulated system was allowed to equilibrate, would each of the phenyl rings maintain their respective parallel and perpendicular modes? Second, could energetics derived from the equilibrated systems suggest why different solvents induce a preferred orientation of the phenyl ring?

To answer these two questions, two frameworks that had phenyl rings in a parallel mode (**3** and **6**) and two frameworks that had phenyl rings in a perpendicular mode (**5** and **7**) were simulated using classical molecular dynamics in LAMMPS with the parameters of the Universal Force Field (UFF).[45,46] The initial structure of each simulated MOF system was obtained through X-ray diffraction. The simulations were then performed with a Lennard-Jones cutoff of 15.0 Å. Each simulation was equilibrated for 0.5 ns. Additional details about the simulations can be found in the Supporting Information.

From simulations performed in the isobaric−isothermal (*NpT*) ensemble at 100 K and 1 atm, deviations from the experimental structure can be compared for both the lattice parameters of the unit cell and the root-mean-square (RMS) displacements of individual atoms. A comparison of the shapes and sizes of the unit cells for the experimental systems and *NpT* simulations shows minor distortions of any given lattice angle (5% or less) and lattice vector (13% or less) (Table S1 in the Supporting Information). In addition to the lattice parameters of the cell, the RMS atomic displacements allow us to gauge the precision of the simulations (Table S2 in the Supporting Information). A visual depiction of the simulations shows that MOFs **3** and **6** with parallel phenyl rings more closely adhere to their single-crystal X-ray structures than MOFs **5** and **7** with perpendicular phenyl rings (Figure 10 and Figures S21−S28 in the Supporting Information). These depictions show instantaneous snapshots of equilibrated structures at 100 K. Overall, these two results suggest that the potential employed is capable of capturing the structure of the framework effectively.

Having established that the simulations can capture the overall structure of the MOFs, we evaluated the rotation of the phenyl rings versus their experimental values. The simulations of MOFs with parallel phenyl rings (**3** and **6**) experimentally show an alternating pattern of positive and negative angles with a magnitude just larger than 20° (Table S3 in the Supporting Information). The materials with perpendicular phenyl rings, experimentally 90° for **5** and 78° for **7**, display smaller angles of 71° and 49°, respectively. The comparison of the experimental and simulated results of the ring rotation can be seen in Figure 11. Overall, the UFF potential produces results that are consistently off from the experimentally observed rotations by about 20°, but notably, the trend of parallel or perpendicular rotation is correctly reproduced in all cases.

Since the simulations correctly reproduced the ring rotation as a function of solvent, we investigated the interaction energies to determine whether a rationale could be devised for the phenyl ring orientation. Energies of interaction between groups of atoms are reported in Table S4 in the Supporting Information on a per unit cell basis. The interaction energies

dx.doi.org/10.1021/ja4088709 | J. Am. Chem. Soc. 2014, 136, 671−678

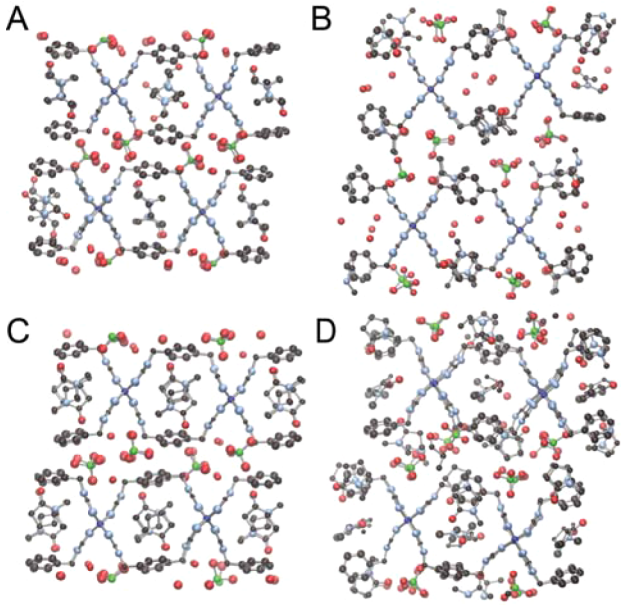

Figure 10. Graphical representations of portions of the equilibrated structures of (A) **3**, (B) **5**, (C) **6**, and (D) **7**. The pictures display instantaneous snapshots of equilibrated structures at 100 K.

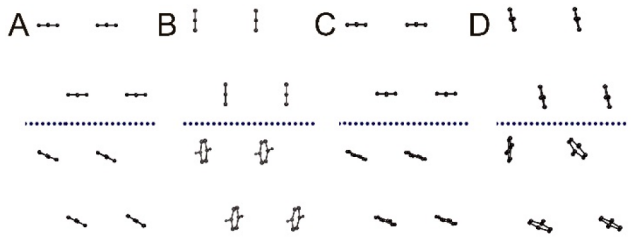

Figure 11. Initial and equilibrated phenyl ring positions for **3** (A), **5** (B), **6** (C), and **7** (D). Initial positions (experimental) are above dotted lines while equilibrated positions (simulated) are below the dotted lines.

are similar within the two categories of ring rotations, suggesting that the energy gap between the two ring positions is small. Essentially, the rotation of the phenyl ring from a parallel orientation to a perpendicular orientation occurs at the cost of framework–framework energy, which is offset by stronger framework–solvent energetic interactions. The anion position also impacts the position of the phenyl rings in a more limited manner. A secondary increase in framework–anion energy and a secondary decrease in anion–solvent energy indicate that the choice of solvent not only impacts the orientation of the phenyl ring but also the position of the anion.

To further understand the effects of the surrounding atoms on the phenyl ring itself, the energies of interaction between the four rotating atoms of the phenyl ring and other surrounding groups of atoms were calculated (Table 1). These results explicitly highlight that the phenyl interaction with the rest of the framework becomes less favorable as the phenyl ring rotates to a perpendicular orientation but also that a more favorable interaction between the phenyl ring and the solvent compensates for this energetic penalty. Solvents that have strong interactions with the phenyl ring favor rotation to the perpendicular orientation, while solvents with weak interactions favor a parallel mode.

Table 1. Lennard-Jones Energies of Interaction between Phenyl Rings and Surrounding Groups of Atoms (kcal/mol per unit cell)

	3	5	6	7
phenyl/framework	−9.3	−2.6	−9.6	−3.2
phenyl/solvent	−8.6	−13.6	−11.2	−19.8
phenyl/anion	−6.4	−3.9	−6.4	−4.3
phenyl/water	−1.1	−1.6	−1.1	–

3. CONCLUSION

A series of two-dimensional MOFs that display a topology of fused 1D metal–organic nanotubes was synthesized, and the frameworks were found to undergo two different transformations in the solid state as a function of solvation. A semirigid bis(1,2,4-triazole) ligand connects one-dimensional copper chains through a syn conformation to form a tubular architecture. The phenyl rings between the 1,2,4-triazoles are oriented either parallel or perpendicular to the tube. The first transformation involves expansion or contraction of the 2D sheet layers as a function of DMF concentration. More notably, DMA and NMP cause the phenyl ring to rotate to an orientation perpendicular to the tube orientation. All of these framework transformations were initially determined by single-crystal X-ray diffraction and powder X-ray diffraction. Since the breathing mode of phenyl rotation is solely ligand-based, we believed that solid-state ^{13}C CP-MAS NMR spectroscopy would be a powerful tool to elucidate this switching mechanism between the parallel and perpendicular modes of the phenyl ring. Unlike PXRD, solid-state ^{13}C CP-MAS NMR spectroscopy could directly monitor phenyl rotation as a function of solvation, demonstrating that this is an effective approach for monitoring changes to a breathing framework that occur solely through gate switching of the ligand. Finally, simulations showed that rotation of the phenyl ring from a parallel orientation to a perpendicular orientation occurs at the cost of framework–framework energy and that this energetic cost is offset by stronger framework–solvent interactions. Future research will focus on preparing isostructural 2D sheet MOFs with functionalized or extended linkers to investigate the effect of pore size on aryl subunit rotation.

■ ASSOCIATED CONTENT

Ⓢ Supporting Information

Detailed synthesis and characterization of all compounds, including TGA, PXRD, NMR, and crystallography; crystallographic data (CIF); procedures for transformations in the solid state; and computational details, including simulation tables and figures. This material is available free of charge via the Internet at http://pubs.acs.org.

■ AUTHOR INFORMATION

Corresponding Author

jenkins@ion.chem.utk.edu

Notes

The authors declare no competing financial interest.

■ ACKNOWLEDGMENTS

We are grateful to the State of Tennessee's Science Alliance, whose JDRD Grant provided partial support for this research.

REFERENCES

(1) Horike, S.; Shimomura, S.; Kitagawa, S. *Nat. Chem.* **2009**, *1*, 695−704.
(2) Kitagawa, S.; Matsuda, R. *Coord. Chem. Rev.* **2007**, *251*, 2490−2509.
(3) Férey, G. *Chem. Soc. Rev.* **2008**, *37*, 191−214.
(4) Uemura, K.; Matsuda, R.; Kitagawa, S. *J. Solid State Chem.* **2005**, *178*, 2420−2429.
(5) Sareeya, B.; Satoru, S.; Susumu, K. *Sci. Technol. Adv. Mater.* **2008**, *9*, No. 014108.
(6) Kitagawa, S.; Kitaura, R.; Noro, S. *Angew. Chem., Int. Ed.* **2004**, *43*, 2334−2375.
(7) Férey, G.; Serre, C. *Chem. Soc. Rev.* **2009**, *38*, 1380−1399.
(8) Kole, G. K.; Vittal, J. J. *Chem. Soc. Rev.* **2013**, *42*, 1755−1775.
(9) Férey, G. *Dalton Trans.* **2009**, 4400−4415.
(10) Férey, G. *Z. Anorg. Allg. Chem.* **2012**, *638*, 1897−1909.
(11) Dhotel, A.; Chen, Z.; Delbreilh, L.; Youssef, B.; Saiter, J. M.; Tan, L. *Int. J. Mol. Sci.* **2013**, *14*, 2303−2333.
(12) Khan, N. A.; Hasan, Z.; Jhung, S. H. *J. Hazard. Mater.* **2013**, *244*−*245*, 444−456.
(13) Kitaura, R.; Seki, K.; Akiyama, G.; Kitagawa, S. *Angew. Chem., Int. Ed.* **2003**, *42*, 428−431.
(14) Llewellyn, P. L.; Bourrelly, S.; Serre, C.; Filinchuk, Y.; Férey, G. *Angew. Chem., Int. Ed.* **2006**, *45*, 7751−7754.
(15) Henke, S.; Schneemann, A.; Wütscher, A.; Fischer, R. A. *J. Am. Chem. Soc.* **2012**, *134*, 9464−9474.
(16) Thallapally, P. K.; Tian, J.; Kishan, M. R.; Fernandez, C. A.; Dalgarno, S. J.; McGrail, P. B.; Warren, J. E.; Atwood, J. L. *J. Am. Chem. Soc.* **2008**, *130*, 16842−16843.
(17) Fletcher, A. J.; Thomas, K. M.; Rosseinsky, M. J. *J. Solid State Chem.* **2005**, *178*, 2491−2510.
(18) Kitagawa, S.; Uemura, K. *Chem. Soc. Rev.* **2005**, *34*, 109−119.
(19) Murdock, C. R.; Lu, Z.; Jenkins, D. M. *Inorg. Chem.* **2013**, *52*, 2182−2187.
(20) Li, X.-L.; Liu, G.-Z.; Xin, L.-Y.; Wang, L.-Y. *CrystEngComm* **2012**, *14*, 5757−5760.
(21) Husain, A.; Ellwart, M.; Bourne, S. A.; Ohrstrom, L.; Oliver, C. L. *Cryst. Growth Des.* **2013**, *13*, 1526−1534.
(22) Park, I.-H.; Lee, S. S.; Vittal, J. J. *Chem.—Eur. J.* **2013**, *19*, 2695−2702.
(23) Horike, S.; Matsuda, R.; Tanaka, D.; Matsubara, S.; Mizuno, M.; Endo, K.; Kitagawa, S. *Angew. Chem., Int. Ed.* **2006**, *45*, 7226−7230.
(24) Gould, S. L.; Tranchemontagne, D.; Yaghi, O. M.; Garcia-Garibay, M. A. *J. Am. Chem. Soc.* **2008**, *130*, 3246−3247.
(25) Winston, E. B.; Lowell, P. J.; Vacek, J.; Chocholousova, J.; Michl, J.; Price, J. C. *Phys. Chem. Chem. Phys.* **2008**, *10*, 5188−5191.
(26) Seo, J.; Matsuda, R.; Sakamoto, H.; Bonneau, C.; Kitagawa, S. *J. Am. Chem. Soc.* **2009**, *131*, 12792−12800.
(27) Yang, W.; Davies, A. J.; Lin, X.; Suyetin, M.; Matsuda, R.; Blake, A. J.; Wilson, C.; Lewis, W.; Parker, J. E.; Tang, C. C.; George, M. W.; Hubberstey, P.; Kitagawa, S.; Sakamoto, H.; Bichoutskaia, E.; Champness, N. R.; Yang, S.; Schroder, M. *Chem. Sci.* **2012**, *3*, 2993−2999.
(28) Murdock, C. R.; Lu, Z.; Jenkins, D. M. *Dalton Trans.* **2012**, *41*, 7839−7841.
(29) Horváth, A. *Synthesis* **1995**, 1183−1189.
(30) Coronado, E.; Gimenez-Marques, M.; Espallargas, G. M. *Inorg. Chem.* **2012**, *51*, 4403−4410.
(31) Kanoh, H.; Kondo, A.; Noguchi, H.; Kajiro, H.; Tohdoh, A.; Hattori, Y.; Xu, W. C.; Inoue, M.; Sugiura, T.; Morita, K.; Tanaka, H.; Ohba, T.; Kaneko, K. *J. Colloid Interface Sci.* **2009**, *334*, 1−7.
(32) Kajiro, H.; Kondo, A.; Kaneko, K.; Kanoh, H. *Int. J. Mol. Sci.* **2010**, *11*, 3803−3845.
(33) Hong, M.; Zhao, Y.; Su, W.; Cao, R.; Fujita, M.; Zhou, Z.; Chan, A. S. *Angew. Chem., Int. Ed.* **2000**, *39*, 2468−2470.
(34) Dong, Y. B.; Jiang, Y. Y.; Li, J.; Ma, J. P.; Liu, F. L.; Tang, B.; Huang, R. Q.; Batten, S. R. *J. Am. Chem. Soc.* **2007**, *129*, 4520−4521.
(35) Ren, S.-B.; Yang, X.-L.; Zhang, J.; Li, Y.-Z.; Zheng, Y.-X.; Du, H.-B.; You, X.-Z. *CrystEngComm* **2009**, *11*, 246−248.
(36) Thanasekaran, P.; Luo, T. T.; Lee, C. H.; Lu, K. L. *J. Mater. Chem.* **2011**, *21*, 13140−13149.
(37) Serre, C.; Millange, F.; Thouvenot, C.; Nogues, M.; Marsolier, G.; Louer, D.; Férey, G. *J. Am. Chem. Soc.* **2002**, *124*, 13519−13526.
(38) Dybtsev, D. N.; Chun, H.; Kim, K. *Angew. Chem., Int. Ed.* **2004**, *43*, 5033−5036.
(39) Demessence, A.; Long, J. R. *Chem.—Eur. J.* **2010**, *16*, 5902−5908.
(40) Hoffmann, H.; Debowski, M.; Müller, P.; Paasch, S.; Senkovska, I.; Kaskel, S.; Brunner, E. *Materials* **2012**, *5*, 2537−2572.
(41) Sutrisno, A.; Huang, Y. *Solid State Nucl. Magn. Reson.* **2013**, *49*−*50*, 1−11.
(42) Rabone, J.; Yue, Y.-F.; Chong, S. Y.; Stylianou, K. C.; Bacsa, J.; Bradshaw, D.; Darling, G. R.; Berry, N. G.; Khimyak, Y. Z.; Ganin, A. Y.; Wiper, P.; Claridge, J. B.; Rosseinsky, M. J. *Science* **2010**, *329*, 1053−1057.
(43) Stylianou, K. C.; Rabone, J.; Chong, S. Y.; Heck, R.; Armstrong, J.; Wiper, P. V.; Jelfs, K. E.; Zlatogorsky, S.; Bacsa, J.; McLennan, A. G.; Ireland, C. P.; Khimyak, Y. Z.; Thomas, K. M.; Bradshaw, D.; Rosseinsky, M. J. *J. Am. Chem. Soc.* **2012**, *134*, 20466−20478.
(44) Lee, E. Y.; Jang, S. Y.; Suh, M. P. *J. Am. Chem. Soc.* **2005**, *127*, 6374−6381.
(45) Rappe, A. K.; Casewit, C. J.; Colwell, K. S.; Goddard, W. A., III; Skiff, W. M. *J. Am. Chem. Soc.* **1992**, *114*, 10024−10035.
(46) Plimpton, S. *J. Comput. Phys.* **1995**, *117*, 1−19.